Spectral Longwave Emission in the Tropics: FTIR Measurement at the Sea Surface and Comparison with Fast Radiation Codes*

DAN LUBIN

California Space Institute, University of California, San Diego, La Jolla, California

DAVID CUTCHIN AND WILLIAM CONANT

Scripps Institution of Oceanography, University of California, San Diego, La Jolla, California

HARTMUT GRASSL

Max-Planck-Institut für Meteorologie, Hamburg, Germany

ULRICH SCHMID AND WERNER BISELLI

Meteorologisches Institut, Universität Hamburg, Hamburg, Germany

(Manuscript received 10 January 1994, in final form 20 May 1994)

ABSTRACT

Longwave emission by the tropical western Pacific atmosphere has been measured at the ocean surface by a Fourier Transform Infrared (FTIR) spectroradiometer deployed aboard the research vessel *John Vickers* as part of the Central Equatorial Pacific Experiment. The instrument operated throughout a Pacific Ocean crossing, beginning on 7 March 1993 in Honiara, Solomon Islands, and ending on 29 March 1993 in Los Angeles, and recorded longwave emission spectra under atmospheres associated with sea surface temperatures ranging from 291.0 to 302.8 K. Precipitable water vapor abundances ranged from 1.9 to 5.5 column centimeters. Measured emission spectra (downwelling zenith radiance) covered the middle infrared ($5-20\ \mu m$) with one inverse centimeter spectral resolution. FTIR measurements made under an entirely clear field of view are compared with spectra generated by LOWTRAN 7 and MODTRAN 2, as well as downwelling flux calculated by the NCAR Community Climate Model (CCM-2) radiation code, using radiosonde profiles as input data for these calculations.

In the spectral interval 800–1000 cm^{-1}, these comparisons show a discrepancy between FTIR data and MODTRAN 2 having an overall variability of 6–7 mW m^{-2} sr^{-1} cm and a concave shape that may be related to the representation of water vapor continuum emission in MODTRAN 2. Another discrepancy appears in the spectral interval 1200–1300 cm^{-1}, where MODTRAN 2 appears to overestimate zenith radiance by 5 mW m^{-2} sr^{-1} cm. These discrepancies appear consistently; however, they become only slightly larger at the highest water vapor abundances. Because these radiance discrepancies correspond to broadband (500–2000 cm^{-1}) flux uncertainties of around 3 W m^{-2}, there appear to be no serious inadequacies with the performance of MODTRAN 2 or LOWTRAN 7 at high atmospheric temperatures and water vapor abundances. On average, CCM-2 flux calculations agree to within 1 W m^{-2} with downwelling flux estimates from the FTIR data over all sea surface temperatures, although this result has a scatter of ±12 W m^{-2} at high sea surface temperatures.

1. Introduction

As a result of current concern about a global warming scenario, considerable interest and research into the basic physics of climate has centered around the western Pacific. This is due to the climate extrema that persist in the region, including the warmest sea surface

temperatures and largest water vapor abundances in the troposphere. Ramanathan and Collins (1991) have proposed a "thermostat" hypothesis, whereby the anvil cirrus resulting from deep convection allows the tropical atmosphere to cool, thereby regulating the atmospheric greenhouse effect and, hence, controlling maximum sea surface temperatures. From late February through early April 1993, the Central Equatorial Pacific Experiment (CEPEX) was carried out under the auspices of the University Corporation for Atmospheric Research (with support from the National Science Foundation and the U.S. Department of Energy) to critically examine various components of the thermostat hypothesis and, more generally, to investigate

the various mechanisms that regulate tropical sea surface temperatures.

A key factor in our understanding of climate processes and in our ability to model climate change is an accurate knowledge of infrared radiative transfer in the earth's atmosphere, as this constitutes the physical basis for the greenhouse effect. For climate physics, the most important greenhouse gas is water vapor due to its widely varying abundance in the atmosphere and its numerous strong absorption features throughout the infrared. Over the tropical Pacific Ocean, deep convection gives rise to large tropospheric water vapor abundances (often as large as 6–7 precipitable centimeters), and in this region a "super greenhouse" effect has been described from the vantage point of space (Vonder Haar 1986; Raval and Ramanathan 1989; Ramanathan and Collins 1991; Hallberg and Inamdar 1993).

Raval and Ramanathan (1989) have demonstrated the importance of both water vapor line absorption and water vapor continuum absorption in the middle infrared. The precise strength of the water vapor continuum is still an unresolved issue and perhaps has an uncertainty of 20% (Briegleb 1992). Grant (1990) has reviewed current empirical knowledge of mid-IR continuum absorption and recommends further improvements in laboratory measurement accuracy. The most current theoretical research tends to discount the importance of the dimer phase in the 8–13 μm spectral region (e.g., Thomas and Nordstrom 1985; Slanina 1988), yet models that emphasize collisional broadening effects on the far wings of water vapor lines still have trouble explaining the negative temperature dependence of the continuum absorption (Grant 1990). Some recent experimental work has suggested that the dimer phase becomes important in the 15–25-μm spectral region (Devir et al. 1994). Kiehl and Briegleb (1992a) have shown that a 20% uncertainty in the continuum absorption strength may result in downwelling surface-flux uncertainties of 5–10 W m^{-2} in the Tropics.

As part of CEPEX, the Fourier Transform Infrared (FTIR) spectroradiometer belonging to the California Space Institute (CalSpace) was deployed aboard the R/V *John Vickers* and was operated throughout a Pacific Ocean crossing beginning at Honiara, Solomon Islands, on 7 March 1993 and ending in Los Angeles, California, on 29 March 1993. The CalSpace FTIR spectroradiometer measured zenith radiance emitted by the atmosphere throughout the middle infrared (500–2000 cm^{-1}) and with a resolution of 1 cm^{-1}. The operation of this instrument has been discussed by Lubin (1994), and experimental details relevant to the CEPEX cruise are given in the appendix. The CEPEX data are now in the public domain and are available from the Office of Field Projects Support at the University Corporation for Atmospheric Research in Boulder, Colorado.

The FTIR experiment during CEPEX had three major scientific objectives. The first objective was to obtain enough atmospheric emission spectra under clear skies to document the large variability in water vapor opacity and to provide a dataset that might be useful to validate radiation codes used in climate models. Second, the FTIR experiment was to investigate the role of anvil cirrus in the tropical longwave radiation budget and to quantify the "f factor," the fraction of the cloud longwave forcing measurable at the surface (Ramanathan and Collins 1991). A third objective was to determine the longwave optical properties of the various cloud types that commonly occur over the Pacific Ocean, including cirrus, altostratus, stratus, and trade cumulus (e.g., Smith et al. 1993; Lubin 1994). The first objective is the focus of this paper.

The cruise proceeded along the latitude 2°S until Christmas Island, Republic of Kiribati, then at 2°N until 213°E, at which point the ship headed directly for Los Angeles. Figure 1 shows the location of the FTIR measurements, highlighting the clear-sky cases. A total of 62 clear-sky emission spectra are used in this study. Ancillary data include atmospheric temperature and water vapor profiles for the troposphere and lower stratosphere, obtained from Vaisala radiosondes provided aboard ship by the Max Planck Institute for Meteorology, and sea surface temperature data recorded as part of the standard shipboard data acquisition system. FTIR measurements were made several times daily, typically every half hour during daylight, and sea surface temperatures were logged during each FTIR measurement. Four radiosondes were launched per day at precisely 0000, 0600, 1200, and 1800 UTC.

We compared the radiances measured by the CalSpace FTIR Spectroradiometer to radiances and fluxes computed by three widely used radiative transfer models that are sufficiently or nearly fast enough to be incorporated into climate model simulations. The fastest algorithm we consider is the National Center for Atmospheric Research (NCAR) Community Climate Model (CCM-2) radiation code (Kiehl and Briegleb 1992b), which was specifically developed for use in a general circulation model. The CCM-2 code treats the mid-IR water vapor line and continuum absorption using the temperature-dependent emissivity and absorptivity formulation developed by Ramanathan and Downey (1986). We also consider LOWTRAN 7, the current version of a well-tested Air Force Geophysics Laboratory (AFGL) model that has been used throughout the atmospheric science community for two decades (Kneizys et al. 1988). LOWTRAN 7 has recently been incorporated into a large-scale radiation budget study by Hallberg and Inamdar (1993) and Inamdar and Ramanathan (1994). The CCM-2 code computes only broadband flux at the surface (integral over 0–2200 cm^{-1}). LOWTRAN 7 computes radiance in any direction with a spectral resolution of 20 cm^{-1}, from which downwelling flux may be computed using
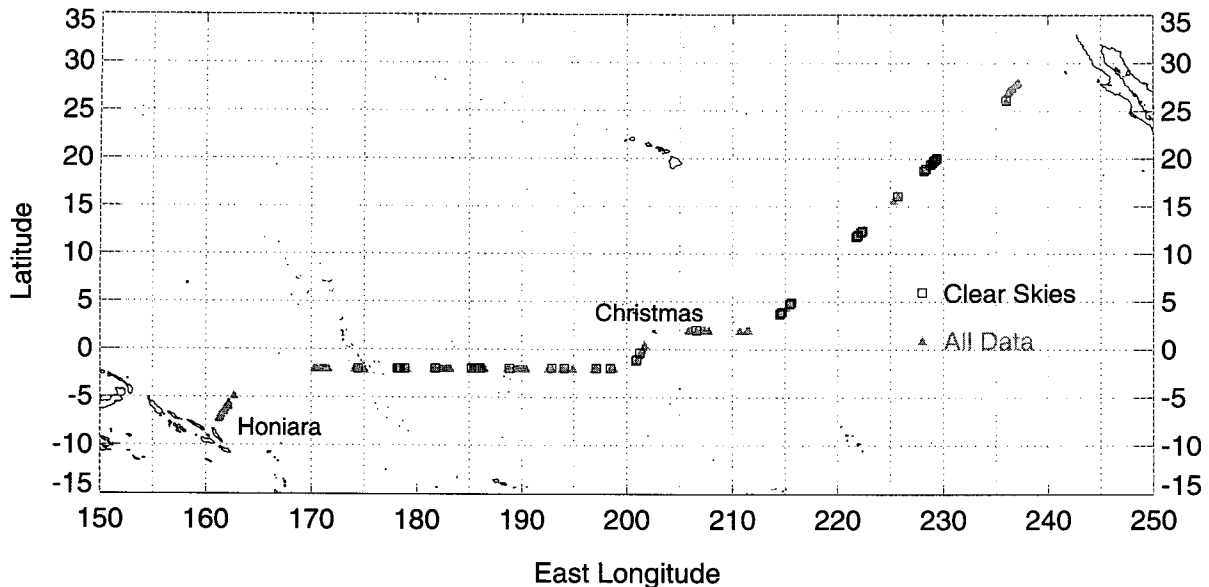
CEPEX FTIR DATA: R/V VICKERS

FIG. 1. Location of CalSpace FTIR spectroradiometer measurements made aboard the R/V *Vickers* during the Central Equatorial Pacific Experiment.

Gaussian quadrature (Chandrasekhar 1960). We also compare the FTIR data with MODTRAN 2 (Berk et al. 1989), a recent AFGL development that computes radiance in a similar fashion as LOWTRAN 7 but contains a parameterization of the entire AFGL HITRAN
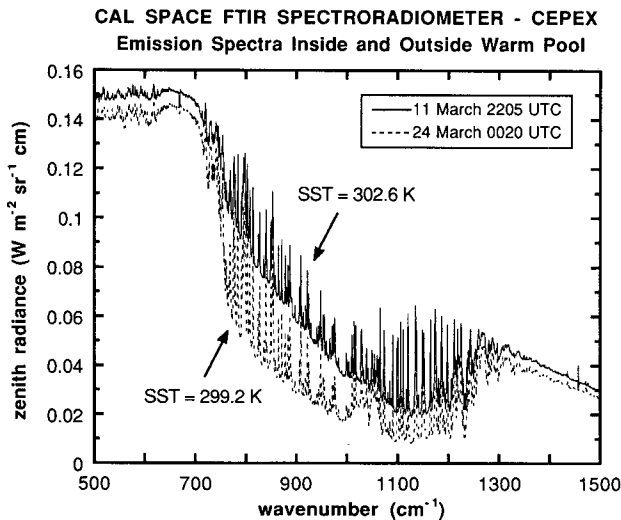

FIG. 2. Examples of atmospheric emission spectra measured by the CalSpace FTIR spectroradiometer during CEPEX. The upper (solid) curve was recorded within the western Pacific warm pool region at 2°0'S, 178°18'E, where the sea surface temperature was 302.6 K; the lower (dotted) curve was recorded outside of the warm pool region at 11°50'N, 222°48'E, where the sea surface temperature was 299.2 K.

atmospheric absorption line parameter database (Rothman et al. 1987) at 2 cm^{-1} spectral resolution. Considerable insight into mid-IR radiative transfer fundamentals can also be gained by comparing FTIR data with AFGL's Fast Atmosphere Signature Code (FASCODE) (e.g., Ellingson et al. 1993). However, because FASCODE operates individually on each relevant molecular transition in the HITRAN database, it is so central processing unit intensive as to be inappropriate for climate model simulation and is not discussed in this report.

2. FTIR data under clear skies

All spectra considered here were recorded under a clear overhead sky with visual determination that there was no cloud cover in the instrument's field of view during the measurement integration time. These measurements pertain to a wide range of sea surface temperatures (291.0–302.8 K). Figure 2 shows two examples of emission spectra recorded under clear skies during the CEPEX cruise. The lower (dotted) curve was recorded east of the "warm pool" region under a humid atmosphere (water vapor column abundance approximately 2.6 cm) and moderate sea surface temperature (299.2 K). The upper (solid) curve was recorded inside the warm pool region (water vapor column abundance 4.9 cm, sea surface temperature 302.6 K) and shows a radiance enhancement of 50% or larger throughout the spectral interval 750–1250 cm^{-1}.

To demonstrate the impact of this variability in opacity on surface longwave fluxes, we transform the

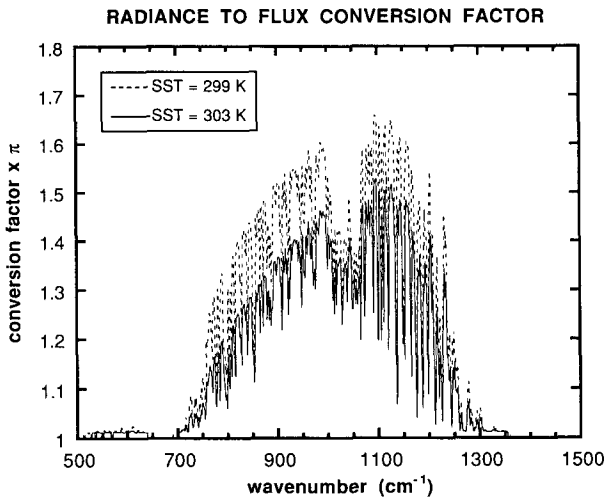**RADIANCE TO FLUX CONVERSION FACTOR**

FIG. 3. Examples of MODTRAN-generated conversion spectra for transforming measured zenith radiance into an estimate of downwelling surface flux. The input data for these MODTRAN 2 calculations are radiosonde data obtained over sea surface temperatures of 299 (dotted curve) and 303 K (solid curve).

measured zenith radiance to a downwelling flux by means of a wavenumber-dependent conversion factor. This conversion factor C_ν is estimated by using MODTRAN 2 to generate radiance spectra $I_{\nu i}$ at $N = 4$ Gaussian quadrature angles (Chandrasekhar 1960), from which downwelling flux F_ν is estimated:

$$F_\nu = 2\pi \sum_{i=1}^{N} \alpha_i \mu_i I_{\nu i}, \qquad (1)$$

where α_i and μ_i are the Gaussian weights and cosines of the view zenith angles, respectively. A MODTRAN 2 estimation of the zenith radiance $I_{\nu 0}$ then establishes the conversion factor

$$C_\nu = \frac{F_\nu}{I_{\nu 0}}. \qquad (2)$$

Two of these spectral conversion factors are shown in Fig. 3. In the fully opaque parts of the mid-IR spectrum (650–700 cm^{-1}, 1350 cm^{-1} and longer), we expect the radiation to be isotropic: $C_\nu = \pi$. In the mid-IR window region and in the region of water vapor rotation lines (500–650 cm^{-1}), C_ν becomes increasingly greater than π as atmospheric opacity decreases. The conversion factor is therefore also a function of atmospheric temperature and water vapor abundance. For model atmospheres (and sea surface temperatures) corresponding to the examples of Fig. 2, the conversion factor in the mid-IR window is approximately 10% smaller for the warmer conditions. With the radiosonde and sea surface temperature data, MODTRAN 2 is used to generate conversion factor spectra as a function of sea surface temperature.

Once downwelling flux has been estimated from zenith radiance, the sea surface temperature data are used to estimate the net flux at the surface, where for this purpose we may approximate sea surface emissivity as a blackbody. The net surface flux, as a function of sea surface temperature, is shown in Fig. 4. Each point in this figure refers to a single estimate (FTIR radiance data converted to flux, from which upwelling flux is subtracted) integrated over the measurable wavenumber range (500–2000 cm^{-1}). The points have been subdivided into four categories depending on their longitude, and these categories correspond to the various climate regimes studied by CEPEX. The longitude intervals $174°$–$180°$E and $196°$–$216°$E were climatologically convective regions where deep convection occurred. The region $180°$–$196°$E was climatologically convective but during the cruise exhibited suppressed convection and noticeably less greenhouse trapping than the two surrounding regions. The colder region $216°$–$240°$E was nonconvective and showed the smallest greenhouse trapping. Overall, this figure exhibits a nonlinear increase in net surface flux for sea surface temperatures greater than 300 K.

3. Comparison of FTIR data with radiation models

a. Spectral comparison

MODTRAN 2 is the most detailed model we consider in this study. This recently developed radiative transfer formulation promises to be one of the more versatile tools available to the atmospheric scientist, as it is computationally fast yet yields results comparable to the much larger FASCODE at 2 cm^{-1} spectral resolution. For comparison with MODTRAN 2, it is ac-
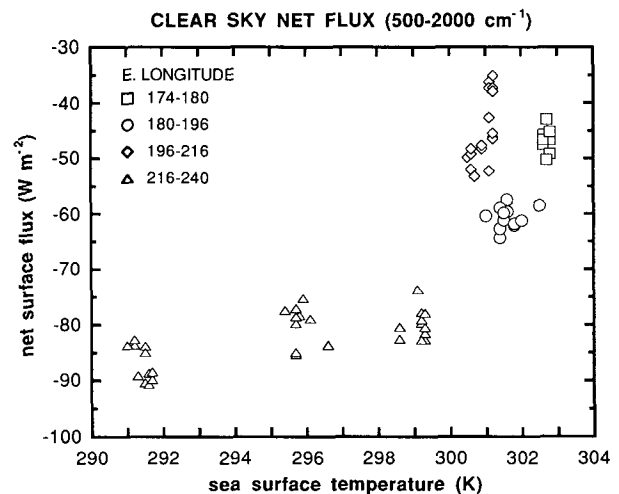
CLEAR SKY NET FLUX (500-2000 cm^{-1})

FIG. 4. Net surface flux under clear skies, as estimated from CalSpace FTIR spectroradiometer data recorded during CEPEX, shown as a function of sea surface temperature. The flux estimates have been sorted into four categories specified by east longitude.
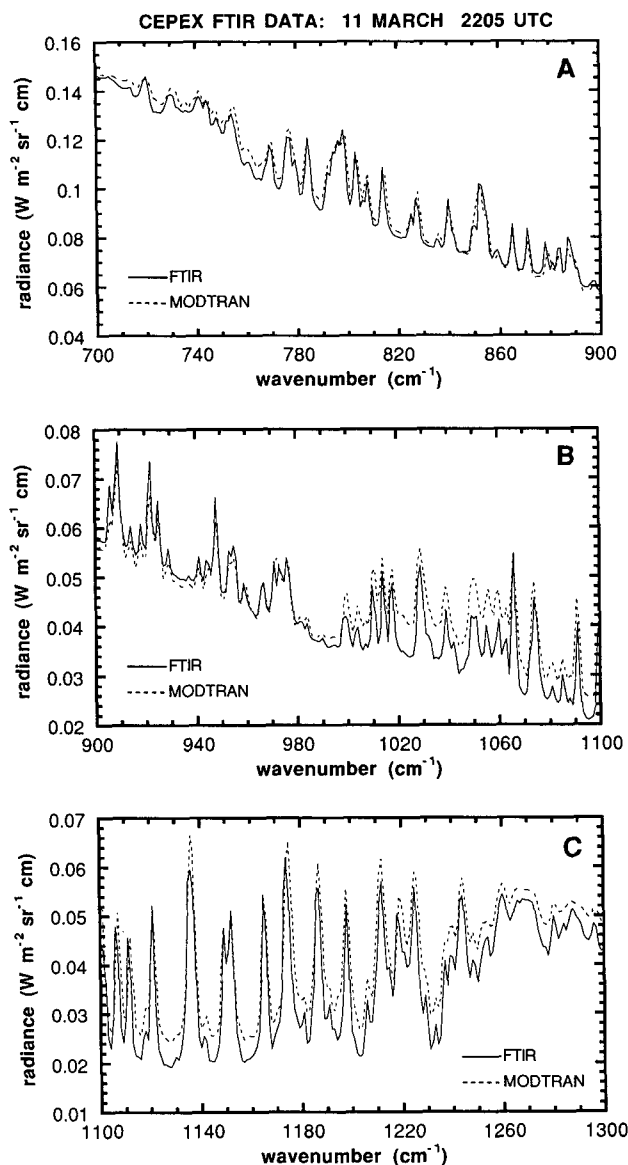
CEPEX FTIR DATA: 11 MARCH 2205 UTC

ent in the FTIR spectrum are reproduced in the MOD-TRAN 2 calculation, indicating that this model contains a complete representation, at 2 cm^{-1} resolution, of mid-IR emission from a tropical atmosphere. The FTIR data as presented here have not been corrected for possible wavenumber errors, and small wavenumber discrepancies appear for several of the emission features. For this study the two most important tasks are 1) verifying that the FTIR data are consistent with MODTRAN 2 in the identification of all emission features, as is shown by Fig. 5, and 2) documenting any differences between the model and data that appear consistently throughout the mid-IR window and that might contribute substantially to uncertainties in flux computation. We have also done a MODTRAN 2 sensitivity study to estimate the possible impact of marine aerosols and have determined that for all reasonable estimates of visibility, maritime aerosols should add no more than 0.5 mW m^{-2} sr^{-1} cm to the spectral zenith radiance throughout the wavenumber interval 800–1400 cm^{-1}.

The second task is more easily addressed by inspecting the difference between a given FTIR zenith radiance spectrum and the MODTRAN 2 spectrum calculated with the radiosonde data nearest in time. Two such difference spectra are shown in Fig. 6, for the examples of Fig. 2. Because we are interested primarily in mid-

FIG. 5. An expanded view of the warm pool emission spectrum of Fig. 2 (solid curve) emphasizing the mid-IR window. The dotted curve denotes a clear-sky MODTRAN 2 calculation using the nearest radiosonde profile.

ceptable to degrade the spectral resolution of the FTIR data to 2 cm^{-1} using a triangular scanning function (G. Anderson 1993, personal communication), and this has been done for all comparisons presented here. One comparison between an FTIR measurement and a MODTRAN 2 calculation is shown in Fig. 5, for the warm pool example of Fig. 2. The MODTRAN 2 calculation was done using the radiosonde data closest in time to the FTIR measurement. Figure 5 has been divided into three panels to better illustrate each of the 2 cm^{-2} resolution water vapor, CO_2, and ozone features throughout the mid-IR window. All such features pres-

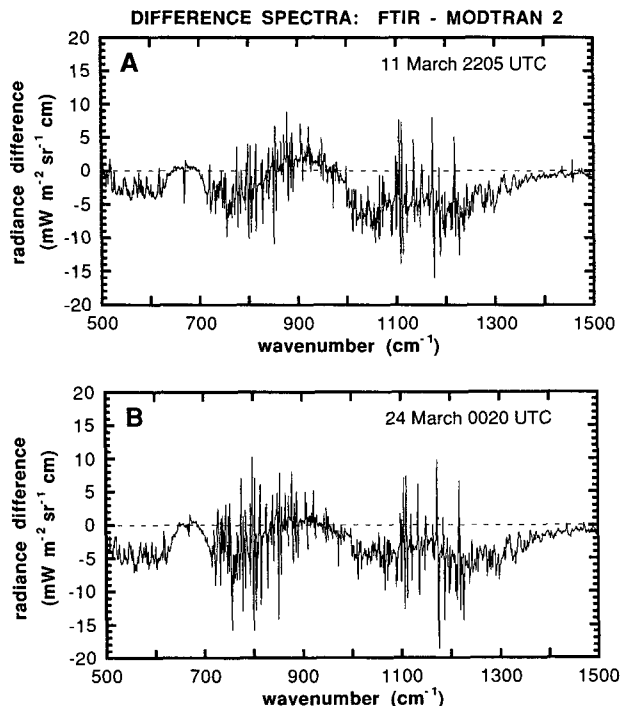**DIFFERENCE SPECTRA: FTIR - MODTRAN 2**

FIG. 6. The difference between a CalSpace FTIR measurement and a MODTRAN 2 calculation using the nearest radiosonde data (a) for the warm pool example of Fig. 2 and (b) for the cooler atmosphere spectrum of Fig. 2. Units are milliwatts per square meter per steradian per inverse centimeter.

IR window emission, the model output and the FTIR data have been normalized in the spectral intervals 625–675 and 1500–2000 cm^{-1} (where we expect the atmosphere to be entirely opaque and, hence, trivially modeled). This normalization was often necessary when the FTIR measurement and the radiosonde launch were more than an hour apart. In the warm pool spectrum (Fig. 6a), we notice that the model appears to overestimate zenith radiance by as much as 5 mW m^{-2} sr^{-1} cm in the spectral interval 770–850 cm^{-1}. Between 850 and 1000 cm^{-1}, the model appears to underestimate the radiance by up to 3 mW m^{-2} sr^{-1} cm. The general concave shape in this discrepancy between 800 and 1000 cm^{-1} may be related to the treatment of water vapor continuum emission in MODTRAN 2. In the spectral interval 1200–1300 cm^{-1}, the model appears to overestimate zenith radiance by approximately 5 mW m^{-2} sr^{-1} cm. In the colder spectrum (Fig. 6b) the concave data model discrepancy appears to be smaller in the interval 800–1000 cm^{-1}, differences ranging from -5 to $+1$ mWm^{-2} sr^{-1} cm, but in the interval 1200–1300 cm^{-1} the discrepancy is nearly the same as for the warm pool example. Discrepancies within the ozone emission band (1000–1080 cm^{-1}) result from incomplete knowledge of the ozone column.

There is one noteworthy discrepancy outside the mid-IR window. Between 500 and 625 cm^{-1}, it appears that MODTRAN 2 overestimates emission from water vapor rotation lines by up to 3 mW m^{-2} sr^{-1} cm on 11 March and by up to 6 mW m^{-2} sr^{-1} cm on 24 March. These discrepancies represent downwelling flux overestimates of approximately 1 and 1.8 W m^{-2} on 11 March and 24 March, respectively.

The largest "spikes" in Figs. 6a,b are due to the small wavenumber offsets mentioned above. With a pronounced emission feature, a small wavenumber error between the model and data will result in the difference spectrum exhibiting two pronounced spikes that are nearly equal in magnitude but opposite in sign and that therefore do not contribute to the integrated radiance difference over the entire window, which is the focus of this study.

Zenith radiance integrated over the spectral interval 800–1000 cm^{-1} is shown in Fig. 7. All clear-sky FTIR measurements are shown in this plot, but the plot highlights those measurements taken close to a radiosonde flight (within one hour before launch or during the ascent). Also shown are zenith radiances computed by both MODTRAN 2 and LOWTRAN 7 from all relevant radiosonde data. The data are plotted as versus water vapor column abundance, which is obtained from the radiosondes. For the smallest water vapor abundances (occuring at the coldest sea surface temperatures), FTIR measurements are generally larger than the model calculations by 0.5 W m^{-2} sr^{-1}. At the largest water vapor abundances (and warmest sea surface temperatures) the discrepancy is typically
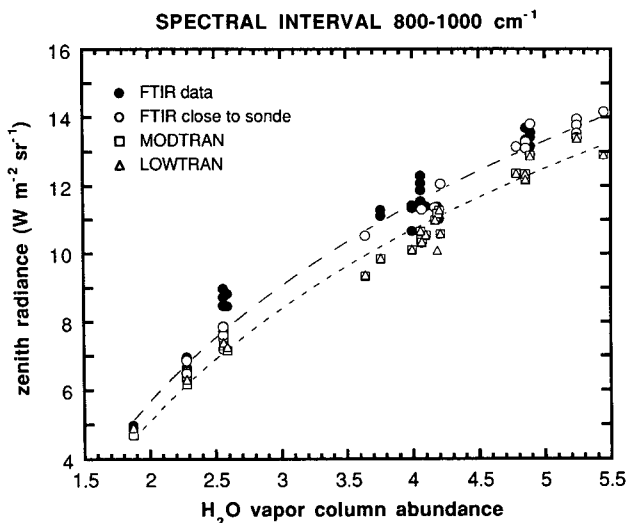

FIG. 7. Zenith radiance integrated over the spectral interval 800–1000 cm^{-1} as measured by the FTIR (circles) and as calculated from the nearest radiosonde data by MODTRAN 2 (open squares) and LOWTRAN 7 (open triangles). Open circles refer to clear-sky FTIR measurements made within one hour before the radiosonde launch or during the radiosonde ascent. Filled circles refer to all other clear-sky FTIR measurements. Precipitable water vapor abundances are calculated from the radiosonde data. The upper, coarsely dashed curve refers to a least-squares logarithmic fit through the FTIR data. The lower, finely dashed curve refers to a least-squares logarithmic fit through the MODTRAN 2 calculations.

1 W m^{-2} sr^{-1}. When transformed to flux, these discrepancies represent model underestimates of 2.3 and 4.2 W m^{-2} for the smallest and largest water vapor abundances, respectively. LOWTRAN 7 and MODTRAN 2 calculations are essentially identical at the largest water vapor abundances but begin to differ by 0.04 W m^{-2} sr^{-1} below 4 cm and are as large as 0.20 W m^{-2} sr^{-1} below 2 cm.

The same information is shown in Fig. 8 for the spectral interval 1200–1400 cm^{-1}. FTIR-measured radiances are consistently smaller than either LOWTRAN 7 or MODTRAN 2 radiances in nearly all cases. This radiance discrepancy appears to be independent of water vapor abundance. The corresponding flux discrepancy in the interval 1200–1400 cm^{-1} is a model overestimate of 1.7 W m^{-2} at the smallest water vapor abundances and a model overestimate of 1.1 W m^{-2} at the largest water vapor abundances. In this spectral interval, LOWTRAN 7 radiances are always smaller than MODTRAN 2 radiances by approximately 0.1 W m^{-2} sr^{-1}.

b. Consistency with previous studies

The radiance discrepancies we notice in Figs. 6a and 6b are representative of the entire clear-sky FTIR dataset from CEPEX. They are consistent in sign with the Spectral Radiation Experiment (SPECTRE) FTIR/
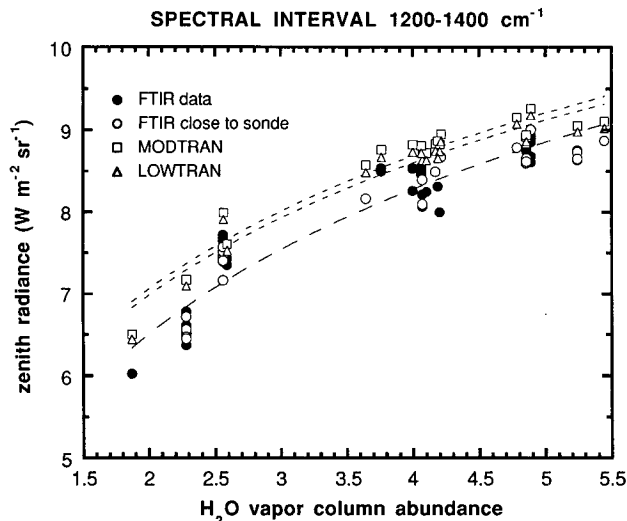
SPECTRAL INTERVAL 1200-1400 cm⁻¹

FIG. 8. As in Fig. 7 but for the spectral interval 1200–1400 cm⁻¹. The lower, coarsely dashed curve refers to a least-squares logarithmic fit through the FTIR data. The two finely dashed curves refer to least-squares logarithmic fits through the MODTRAN 2 (upper curve) and LOWTRAN 7 (middle curve) calculations.

FASCODE intercomparisons of Ellingson et al. (1993) but are 2.5 times larger than the SPECTRE results in the interval 1200–1400 cm⁻¹ and more than 10 times large than the SPECTRE results in the 800–1000-cm⁻¹ interval. This is to be expected, as MODTRAN contains additional approximations beyond those used by FASCODE, to enable fast calculation at 2-cm⁻¹ resolution.

An encouraging comparison between measured FTIR emission spectra and both MODTRAN and FASCODE has been performed by Thériault et al. (1993), who indeed find larger radiance discrepancies for MODTRAN than for FASCODE. Thériault et al. (1993) measured zenith radiance under a water vapor column of 1.8 precipitable centimeters (noticeably drier than most of the atmospheres considered in this study) and found that MODTRAN may overestimate radiance by up to 4 mW m⁻² sr⁻¹ cm between 1200 and 1400 cm⁻¹. In the interval 800–1000 cm⁻¹, they find some individual feature discrepancies as large as 12 mW m⁻² sr⁻¹ cm and an overall variability in the difference spectrum of 4 mW m⁻² sr⁻¹ cm, which exhibits a concave behavior similar to that that we show in Figs. 6a and 6b. Our difference spectra in the interval 500–625 cm⁻¹ are also consistent with Thériault et al. (1993).

c. Comparison of flux estimates

To compare the FTIR data with NCAR CCM-2 output, we must transform the measured radiance to downwelling flux as discussed in section 2, integrate the radiance over the entire measurable mid-IR band

(500–2000 cm⁻¹), and to this add supplemental flux estimates in the spectral intervals 0–500 and 2000–2200 cm⁻¹. Supplemental flux estimates are necessary because CCM-2 output contains no spectral resolution (it computes a broadband flux over 0–2200 cm⁻¹) and because there are no separate radiation measurements from the CEPEX R/V *John Vickers* cruise in the intervals 0–500 and 2000–2200 cm⁻¹. The supplements are therefore provided by LOWTRAN 7 using the appropriate radiosonde data. These two supplemental spectral intervals represent approximately 31% of the total longwave flux but in these intervals the atmosphere is opaque enough that variability in the supplemental flux estimates was no more than 2 W m⁻² over a sea surface temperature range 299–303 K. Hence, there is only a small uncertainty when supplementing the FTIR data with the LOWTRAN 7 estimates, and we expect the largest discrepancies between the data and the models to be associated with mid-IR window emission that the FTIR measures. Estimates of 0–2200-cm⁻¹ downwelling flux from the FTIR data are presented as a function of sea surface temperature in Fig. 9a, along with broadband fluxes computed by both CCM-2 and LOWTRAN 7. The differences between the FTIR-derived flux and CCM-2, and between FTIR-derived flux and LOWTRAN 7, are shown as a function of sea surface temperature in Fig. 9b.

At high sea surface temperatures, LOWTRAN and CCM-2 flux calculations are essentially identical. In colder conditions the two models begin to differ, with slightly larger fluxes for LOWTRAN 7. This discrepancy between models is approximately 2.5 W m⁻² at sea surface temperatures around 300 K, increasing to approximately 6 W m⁻² at sea surface temperatures less than 297 K. The result of this discrepancy, as shown by Fig. 9b, is that the FTIR flux estimates are on average equal to the CCM-2 calculations for all sea surface temperatures, while there is an increasing difference between FTIR flux estimates and LOWTRAN 7 calculations for sea surface temperatures below 297 K. At the highest sea surface temperatures, the FTIR flux estimates agree very well with both CCM-2 and LOWTRAN 7 calculations, although Fig. 9b shows a considerable scatter of ±12 W m⁻².

4. Discussion

This study suggests that current versions of the three fast radiation codes should give very good estimates of downwelling longwave clear-sky flux in the Tropics. When comparing the FTIR emission spectra with MODTRAN zenith radiance calculations, small discrepancies arise in the mid-IR window region. These are a concave difference spectrum with an overall variability of 6–7 mW m⁻² sr⁻¹ cm in the spectral interval 800–1000 cm⁻¹ and a consistent model overestimate of 5 mW m⁻² sr⁻¹ cm in the spectral interval 1200–1300 cm⁻¹. These discrepancies may be due to MOD-

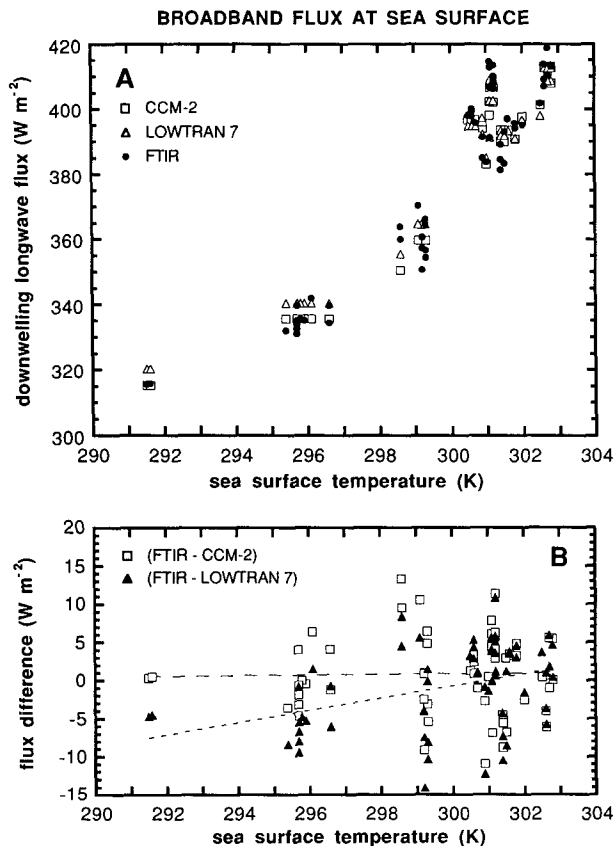## BROADBAND FLUX AT SEA SURFACE

FIG. 9. Downwelling longwave flux at the sea surface (a) as estimated from the CalSpace FTIR data (circles), from the radiosonde data and LOWTRAN 7 (triangles), and from the radiosonde data and the NCAR CCM-2 radiation code (squares); (b) the difference between the FTIR and CCM-2 flux estimates, and the difference between the FTIR and LOWTRAN 7 flux estimates. In (b), the lower, finely dotted line refers to the linear fit through the FTIR–LOWTRAN 7 differences, while the upper, coarsely dotted line refers to the linear fit through the FTIR–CCM-2 differences.

TRAN's treatment of the water vapor continuum absorption. The CEPEX FTIR data pertain to a wide range in tropospheric water vapor burden, and it is worth noting that the model data radiance discrepancies do not increase very much with increasing water vapor column abundance, even in the super greenhouse regime. If the radiances presented in Figs. 6–8 are transformed to flux as discussed in section 2, then MODTRAN 2 and LOWTRAN 7 appear to underestimate mid-IR window flux by approximately 0.6 W m^{-2} over the lowest sea surface temperatures considered here. This underestimate increases to approximately 3.0 W m^{-2} at the highest sea surface temperatures. The model data radiance discrepancies in various parts of the mid-IR window, noted by Figs. 6a and 6b, partly cancel each other. Finally, the LOWTRAN 7 and CCM-2 models compare equally well with the FTIR data, for calculating downwelling surface flux in regions of high sea surface temperature. In re-

gions where the sea surface temperature is colder than 297 K, CCM-2 shows a better comparison with the FTIR data.

This study demonstrates the utility of the CEPEX FTIR dataset and the promise of current Michelson interferometer technology for rigorous field work in extreme climates. The FTIR data presented here suggest that some uncertainties remain in the modeling of water vapor continuum emission in warm, moist atmospheres. However, these data represent a sample of only one month's duration. As discussed in the appendix, the data were also gathered under challenging experimental conditions. Current research (e.g., Ramanathan and Collins 1991) suggests that we must have precise knowledge of clear-sky longwave opacity in order to quantify subtle effects such as the radiative forcing of cirrus clouds. We therefore emphasize that the CEPEX FTIR experiment constitutes only the preliminary investigation of this type, and we encourage an FTIR measurement program in the tropical Pacific having a much longer duration and working in as controlled an environment as possible.

APPENDIX

Radiometric FTIR Experiment

The purpose of this appendix is to demonstrate that the data gathered by the CalSpace FTIR Spectroradiometer during CEPEX are adequate for the stated objectives. The CalSpace FTIR spectroradiometer is based on the Bomem MB-100 Michelson interferometer, configured to view either the zenith sky or a Mikron 340 blackbody calibration source traceable to the National Institute for Standards and Technology (NIST). Each measurement procedure consisted of two scans of the zenith sky and three scans of the blackbody calibration source set at nominal temperatures 5°, 20°, and 30°C. A liquid nitrogen cooled HgCdTe detector enabled the interferometer to operate throughout the middle infrared (500–2000 cm^{-1}) with a resolution of 1 cm^{-1}. In the field, the temperature of the Mikron 340 blackbody element was recorded using a platinum resistance temperature device (RTD) sampled by a Fluke Model 45 digital multimeter. The CalSpace instrument is similar to more elaborate mid-IR spectroradiometers currently in operation as part of the U.S. Department of Energy Atmospheric Radiation Measurement program (e.g., Smith et al. 1993) and has been discussed in greater detail by Lubin (1994).

During CEPEX, the CalSpace FTIR Spectroradiometer was mounted in a gimbaled cradle on the open

quarter-deck of the research vessel *John Vickers*. The vessel's small size necessitated this open air deployment, and throughout the cruise both the interferometer and the blackbody calibration source were exposed to salt air, high air temperature and humidity, and occasional spray. The instrument functioned reliably throughout the cruise, with some deterioration in optical throughput. To operate the instrument on deck, the blackbody RTD calibration cable had to be lengthened and also exposed to the elements. In addition to these experimental challenges, the preseason NIST-traceable adjustments to the blackbody were lost in transit from San Diego to Honiara, and data reduction was accomplished using only postseason calibration information. The absolute radiometric calibration of the CEPEX data was therefore examined as carefully as possible and intercompared with surface air temperature data from both the radiosondes and the ship's data acquisition system. Uncertainty in absolute radiometric calibration (measurement accuracy) was found to be at most $\pm 1°C$ in brightness temperature in the 625–675 cm^{-1} CO$_2$ emission band. This uncertainty corresponds to radiance uncertainties of ± 1.8 mW m^{-2} sr^{-1} cm at wavenumber 800 cm^{-1}, ± 1.6 mW m^{-2} sr^{-1} cm at 1000 cm^{-1}, and ± 1.2 mW m^{-2} sr^{-1} cm at 1250 cm^{-1}. Corresponding uncertainties in estimated downwelling surface flux are ± 3.0 W m^{-2} for the mid-IR window and ± 6.0 W m^{-2} for the measurable longwave (500–2000 cm^{-1}).

Figure A1 illustrates typical performance of the CalSpace FTIR Spectroradiometer during the CEPEX cruise. Instrument responsivity and noise equivalent spectral radiance (NESR, an indication of measurement precision) are shown in Figs. 10a and 10b, respectively. These curves were determined near the end of the cruise and therefore represent the lower bound in instrument performance. The interferometer possessed adequate responsivity throughout the spectral interval 500–2000 cm^{-1}, with maximal responsivity at the short-wavenumber end of the mid-IR window. Throughout the spectral interval 700–1300 cm^{-1}, NESR is at or below 1 mW m^{-2} sr^{-1} cm. (For clarity NESR is expressed here in mW m^{-2} sr^{-1} cm, defined for the specific integration time rather than per root hertz.) We have also inspected the radiometric calibration spectra for anomalous phase contributions from within the interferometer, following Revercomb et al. (1988), and found none. In addition, we inspected the calibrations for linearity in detector response and determined that a possible nonlinearity introduced by blackbody temperatures at or greater than 30°C (Griffiths and de Haseth 1986) results in a radiance uncertainty of less than 1 mW m^{-2} sr^{-1} cm in the mid-IR window, this being a maximum around 1100 cm^{-1}. We therefore conclude that the CEPEX FTIR data are adequate for validating the treatment of water vapor continuum emission in climate model radiation codes.
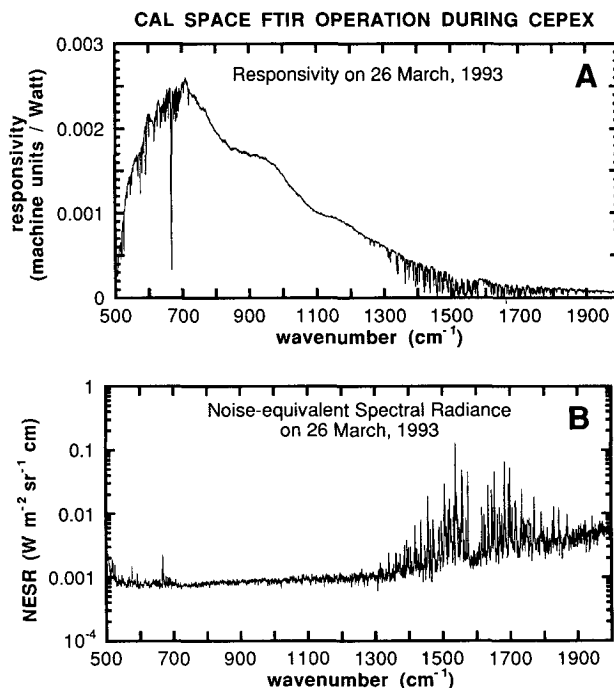

FIG. A1. Examples of CalSpace FTIR spectroradiometer performance during the CEPEX cruise: (a) instrument responsivity near the end of the cruise and (b) noise equivalent spectral radiance near the end of the cruise.

REFERENCES

Berk, A., L. S. Bernstein, and D. C. Robertson, 1989: MODTRAN: A Moderate Resolution Model for LOWTRAN 7. GL-TR-89-0122, Air Force Geophysics Laboratory, Hanscom AFB, 38 pp.

Briegleb, B. P., 1992: Longwave band model for thermal radiation in climate studies. *J. Geophys. Res.*, **97**, 11 475–11 485.

Chandrasekhar, S., 1960: *Radiative Transfer*. Dover, 393 pp.

Devir, A. D., M. Neumann, S. G. Lipson, and U. P. Oppenheim, 1994: Water vapor continuum in the 15- to 25-mm spectral region: Evidence for (H2O)2 in the atmosphere. *Opt. Eng.*, **33**, 746–750.

Ellingson, R. G., and Coauthors, 1993: The Spectral Radiation Experiment (SPECTRE): Clear-sky observations and their use in ICRCCM and ITRA. *IRS 1992: Current Problems in Atmospheric Radiation*, S. Keevallik and O. Karner, Eds., A. Deepak, 451–453.

Grant, W. B., 1990: Water vapor absorption coefficients in the 8–13-μm spectral region: A critical review. *Appl. Opt.*, **29**, 451–462.

Griffiths, P. R., and J. A. de Haseth, 1986: *Fourier Transform Infrared Spectroscopy*. John Wiley and Sons, 656 pp.

Hallberg, R., and A. K. Inamdar, 1993: Observations of seasonal variations in atmospheric greenhouse trapping and its enhancement at high sea surface temperature. *J. Climate*, **6**, 920–931.

Inamdar, A. K., and V. Ramanathan, 1994: Physics of greenhouse effect and convection in warm oceans. *J. Climate*, **7**, 715–731.

Kiehl, J. T., and B. P. Briegleb, 1992a: Comparison of the observed and calculated clear sky greenhouse effect: Implications for climate studies. *J. Geophys. Res.*, **97**, 10 037–10 049.

——, and ——, 1992b: CCM-2 Radiation Column Model FORTRAN computer code, National Center for Atmospheric Research.

Kneizys, F. X., E. P. Shettle, L. W. Abreu, J. H. Chetwynd, G. P. Anderson, W. O. Gallery, J. E. A. Selby, S. A. Clough, and

R. W. Fenn, 1988: Users Guide to LOWTRAN 7. Air Force Geophysics Laboratory, Report AFGL-TR-88-0177, Hanscom AFB, 137 pp.

Lubin, D., 1994: Infrared radiative properties of the maritime Antarctic atmosphere. *J. Climate,* **7,** 121–140.

Ramanathan, V., and P. Downey, 1986: A nonisothermal emissivity and absorptivity formulation for water vapor. *J. Geophys. Res.,* **91,** 8649–8666.

——, and W. Collins, 1991: Thermodynamic regulation of ocean warming by cirrus clouds deduced from observations of the 1987 El Niño. *Nature,* **351,** 27–32.

Raval, A., and V. Ramanathan, 1989: Observational determination of the greenhouse effect. *Nature,* **342,** 758–761.

Revercomb, H. E., H. Buijs, H. B. Howell, D. D. Laporte, W. L. Smith, and L. A. Sromovsky, 1988: Radiometric calibration of IR Fourier transform spectrometers: Solution to a problem with the high-resolution interferometer sounder. *Appl. Opt.,* **27,** 3210–3218.

Rothman, L. S., and Coauthors, 1987: The HITRAN database: 1986 edition. *Appl. Opt.,* **26,** 4085–4097.

Slanina, Z., 1988: A theoretical evaluation of water oligomer population in the earth's atmosphere. *J. Atmos. Chem.,* **6,** 185–190.

Smith, W. L., X. Lin, S. A. Ackerman, H. E. Revercomb, and R. O. Knuteson, 1993: Remote sensing cloud properties from high spectral resolution infrared observations. *J. Atmos. Sci.,* **50,** 1708–1720.

Thériault, J.-M., G. P. Anderson, J. H. Chetwynd, E. Murphy, V. Turner, M. Cloutier, A. Smith, and J.-L. Moncet, 1993: Retrieval of tropospheric profiles from IR emission spectra: Preliminary results with DBIS. *Proc. Soc. Photo-Opt. Instrum. Eng.,* **2049,** 119–128.

Thomas, M. E., and R. J. Nordstrom, 1985: Line shape model for describing infrared absorption by water vapor. *Appl. Opt.,* **24,** 3526–3530.

Vonder Haar, T. H., 1986: Surface radiation budget observations and analysis. Surface radiation budget for climate applications, NASA Reference Publication 1169, 87–101.